

# Fourier Feature Methods for Nonlinear Causal Discovery: FFML Scoring, TRFF Scoring, and FFCI Testing in Mixed Data

Joseph Ramsey  
 Department of Philosophy  
 Carnegie Mellon University  
 Pittsburgh, PA 15213  
 jdramsey@andrew.cmu.edu

## Abstract

Gaussian process (GP) marginal likelihood scores and kernel conditional independence tests are theoretically appealing for nonlinear causal discovery but computationally prohibitive at scale. We present three complementary RFF-based methods forming a practical toolkit for score-based, constraint-based, and hybrid causal discovery.

The Fourier Feature Marginal Likelihood (FFML) score approximates the exact GP marginal likelihood by replacing the  $n \times n$  kernel Gram matrix with a finite-dimensional feature representation, reducing cost to  $O(nm^2 + m^3)$  while retaining the probabilistic interpretation and automatic complexity penalty of the exact score. FFML extends to mixed (continuous and discrete) parent sets via a product-kernel construction, with a Kronecker path for small discrete parent sets and a Hadamard-product path otherwise.

The Tetrad Random Fourier Feature (TRFF) score is a complementary BIC-style alternative using penalized Student-t regression with random Fourier features. TRFF offers robustness to heavy-tailed noise and faster runtime than FFML. Empirically, TRFF and FFML exhibit a complementary precision-recall profile: TRFF achieves higher precision while FFML achieves better recall and lower SHD overall.

The Fourier Feature Conditional Independence (FFCI) test is a fast nonparametric CI test for mixed data, using ridge residualization in feature space and a Frobenius-norm cross-covariance statistic approximated as a weighted sum of chi-squared variables. Empirically, BOSS+FFML achieves the lowest SHD on nonlinear data, while BOSS+TRFF offers the highest precision. When run through PC-Max, FFCI and RCIT exhibit complementary precision-recall profiles: RCIT is more precise while FFCI achieves better recall and substantially lower SHD, at approximately twice the runtime.

## 1 Background and Motivation

Kernel-based methods provide a principled and flexible approach to modeling nonlinear relationships in causal discovery. They are attractive both for score-based algorithms, which evaluate candidate parent sets via regression-style objectives, and for constraint-based algorithms, which rely on conditional independence (CI) testing. In greedy score-based search procedures such as FGES [Ramsey et al., 2017] and BOSS [Andrews et al., 2023], the score must be *stable* under small changes to the parent set, *local* in the sense that it decomposes by variable, and *comparable across parent sets* of differing size and composition.

## 1.1 Kernel Scores for Causal Discovery

Gaussian process (GP) marginal likelihoods satisfy these desiderata and serve as natural nonlinear generalizations of linear-Gaussian scores. By integrating out the regression function, GP marginal likelihoods provide an automatic complexity penalty and behave smoothly under parent additions and deletions. However, exact GP marginal likelihoods require forming and factorizing an  $n \times n$  kernel Gram matrix, leading to  $\mathcal{O}(n^3)$  time and  $\mathcal{O}(n^2)$  memory, which is computationally prohibitive at scale.

Huang et al. [2018] introduced the first practical kernel-based score for causal discovery, demonstrating that nonlinear dependencies could be detected reliably in greedy search without committing to a parametric functional form. Their *generalized score* measures the improvement in kernel ridge regression fit when a candidate parent is added, using residual operators of the form  $(K_Z + \lambda I)^{-2}$ . This construction is a direct inspiration for FFML: both methods use a kernel over the parent set to evaluate the conditional distribution of a child variable, and both are designed to be local and decomposable for use in score-based search.

FFML differs from the Huang et al. score in two important respects. First, FFML approximates the exact GP *marginal likelihood* rather than a regression-residual criterion. The marginal likelihood involves only the single inverse  $(K_Z + \sigma^2 I)^{-1}$  together with a log-determinant normalization, giving it a clean probabilistic interpretation and an automatic Occam factor that penalizes complexity without a separate tuning step. Because the Huang et al. score is derived from regression residuals rather than a joint probabilistic model, it does not carry an analogous complexity penalty, and small parent-set changes can induce larger score fluctuations that reduce stability in greedy search. Second, by replacing the  $n \times n$  Gram matrix with a finite-dimensional RFF representation, FFML reduces cost to  $\mathcal{O}(nm^2 + m^3)$  while retaining this probabilistic interpretation. Finally, neither the Huang et al. score nor the exact GP marginal likelihood supports discrete variables natively; FFML extends to mixed (continuous and discrete) parent sets through a product-kernel construction described in Section 5.

TRFF takes a different approach to the same goal. Rather than approximating a GP marginal likelihood, TRFF fits a Student- $t$  regression model in the random feature space and penalizes complexity via an effective-degrees-of-freedom BIC penalty. This makes TRFF more robust to heavy-tailed noise distributions and faster to compute, at the cost of a less principled complexity penalty. The two scores are compared in detail in Section 8.

## 1.2 Kernel Tests for Conditional Independence

Kernel Conditional Independence (KCI), introduced by Zhang et al. [2012], provides a theoretically principled nonparametric CI test based on the eigenspectrum of kernel Gram matrices. KCI is consistent against all alternatives and requires no parametric assumptions on the joint distribution, making it attractive for constraint-based causal discovery on nonlinear data. However, Strobl et al. [2019] noted that KCI scales at least quadratically with sample size—more precisely  $\mathcal{O}(n^3)$  due to the required eigendecomposition—rendering it unusable for large datasets and making it computationally infeasible at the 20-node,  $n = 2,000$  setting we consider in our experiments.

Strobl et al. [2019] introduced the Randomized Conditional Independence Test (RCIT) as a scalable approximation to KCI, replacing the exact Gram matrices with random Fourier feature approximations, reducing cost to linear in  $n$  while approximating the KCI test statistic. RCIT represents an important step toward practical nonparametric CI testing and is a direct predecessor of FFCI.

However, we find that RCIT as implemented in `causal-learn` has two limitations that motivate

FFCI. First, FFCI’s  $p$ -value approximation methods were selected with an eye toward producing well-calibrated, approximately uniform  $p$ -values under the null, making each suitable for use within a causal discovery algorithm at scale. The gamma approximation is recommended as the default. Second, RCIT as implemented in `causal-learn` does not support discrete variables directly.

FFCI addresses both limitations. On the  $p$ -value side, FFCI offers four approximation methods—gamma, saddlepoint, Davies/Imhof, and a faster residual-based permutation procedure—all selected for their ability to produce well-calibrated, approximately uniform  $p$ -values under the null, making each suitable for use within a causal discovery algorithm at scale. The gamma approximation is recommended as the default. On the discrete variable side, FFCI extends to mixed continuous–discrete data through a per-variable feature construction that concatenates RFF/ORF continuous features with a Cholesky-factored categorical feature map for discrete variables, described in Section 6. FFCI additionally uses separate feature counts for the tested variables ( $m_{XY}$ ) and the conditioning set ( $m_Z$ ), allowing a richer representation of the conditioning set where it matters most for test power. In our experiments, RCIT is accessed via a wrapper that calls `causal-learn`’s RCIT implementation [Zheng et al., 2024] and presents it as a Tetrad `IndependenceTest`, so that PC-Max + RCIT and PC-Max + FFCI run through the same Tetrad PC-Max implementation. The two tests differ in both their  $p$ -value approximation methods (Lindsay–Pilla–Basak `1pd4` for RCIT; gamma for FFCI) and their feature counts (100 conditioning-set features and 5 non-conditioning features for RCIT;  $m_Z = 50$  and  $m_{XY} = 10$  for FFCI), so the comparison is not fully controlled on either dimension. Under this comparison, FFCI and RCIT exhibit complementary precision–recall profiles: RCIT achieves higher precision while FFCI achieves better recall and lower SHD, at approximately twice the runtime.

### 1.3 Computational Setting

FFML, TRFF, and FFCI address the computational barriers of their exact counterparts—the GP marginal likelihood and KCI—by replacing  $n \times n$  kernel Gram matrices with finite-dimensional RFF representations whose dimension  $m$  is controlled independently of the sample size. All three methods reduce to  $\mathcal{O}(nm^2)$  per evaluation (with an  $\mathcal{O}(n^3)$  path retained in FFML when two or more discrete parents are present), making them practical at the scales where exact kernel methods are infeasible. Together they form a coherent toolkit: FFML and TRFF for score-based and hybrid search, FFCI for constraint-based search, all resting on the same RFF/ORF approximation philosophy and compatible bandwidth and regularization strategies. Section 2 reviews the exact GP marginal likelihood that FFML approximates; Section 3 describes the RFF/ORF machinery common to all three methods.

## 2 Exact Kernel Marginal Likelihood (KML)

Let  $Y \in \mathbb{R}^n$  be a centered response variable and  $Z \in \mathbb{R}^{n \times d}$  the matrix of parent observations. We model the conditional distribution of  $Y$  given  $Z$  via a Gaussian process:

$$Y = f(Z) + \varepsilon, \quad \varepsilon \sim \mathcal{N}(0, \sigma^2 I_n), \quad f \sim \mathcal{GP}(0, k(\cdot, \cdot)).$$

Let  $K_Z \in \mathbb{R}^{n \times n}$  be the kernel Gram matrix with  $(K_Z)_{ij} = k(z_i, z_j)$ . Integrating out  $f$  yields the marginal covariance  $C = K_Z + \sigma^2 I_n$ , and the GP marginal log-likelihood (up to an additive constant) is:

$$\mathcal{S}_{\text{KML}}(Y | Z) = -\frac{1}{2} Y^\top C^{-1} Y - \frac{1}{2} \log |C|.$$

This score integrates out  $f$  to avoid overfitting, is well-defined even when  $d > n$ , and behaves smoothly under parent additions and deletions. Computing it requires a Cholesky decomposition of  $C$ , costing  $\mathcal{O}(n^3)$  time and  $\mathcal{O}(n^2)$  memory. FFML approximates this score efficiently by replacing  $K_Z$  with a low-rank random feature approximation.

### 3 Random Fourier Feature Approximation

For shift-invariant kernels such as the Gaussian RBF kernel, Bochner’s theorem [Rahimi and Recht, 2007] guarantees a spectral representation:

$$k(z, z') = \mathbb{E}_{\omega, b} \left[ \sqrt{2} \cos(\omega^\top z + b) \sqrt{2} \cos(\omega^\top z' + b) \right],$$

where  $\omega$  is drawn from the spectral measure of  $k$  and  $b \sim \text{Uniform}(0, 2\pi)$ .

We parameterize the Gaussian RBF kernel as  $k(z, z') = \exp(-\|z - z'\|^2/bw^2)$ , so the spectral distribution is  $\omega \sim \mathcal{N}(0, \frac{2}{bw^2}I_d)$ . Using  $m$  random samples  $(\omega_j, b_j)$ , we obtain the feature map:

$$\phi(z) = \sqrt{\frac{2}{m}} \begin{bmatrix} \cos(\omega_1^\top z + b_1) \\ \vdots \\ \cos(\omega_m^\top z + b_m) \end{bmatrix} \in \mathbb{R}^m, \quad k(z, z') \approx \phi(z)^\top \phi(z').$$

Stacking rows gives  $\Phi \in \mathbb{R}^{n \times m}$  with  $K_Z \approx \Phi \Phi^\top$ .

#### 3.1 Orthogonal Random Features (ORF)

Standard RFF draws  $\omega_1, \dots, \omega_m$  independently, which can produce noticeable Monte Carlo variance when  $m$  is modest. *Orthogonal Random Features* (ORF) [Yu et al., 2016] reduce this variance by generating frequencies that form approximately orthogonal directions, spreading coverage more uniformly in  $\mathbb{R}^d$ .

The ORF construction proceeds in blocks of size  $d$ :

- (1) Sample a random Gaussian matrix and extract an orthonormal basis  $Q$  via QR decomposition.
- (2) Sample radii  $r_i \sim \chi(d)$  (the distribution of  $\|g\|$  for  $g \sim \mathcal{N}(0, I_d)$ ).
- (3) Set  $\omega_i = s r_i q_i$ , where  $q_i$  is the  $i$ th row of  $Q$  and  $s = \sqrt{2}/bw$ .

If  $m > d$ , the procedure repeats for additional blocks. Phase offsets  $b_j$  remain i.i.d.  $\text{Uniform}(0, 2\pi)$ . Both FFML, TRFF, and FFCI support RFF and ORF interchangeably; the score and test formulas are unchanged, only the frequency sampling differs. ORF typically yields lower-variance kernel approximations and increased stability of score differences in greedy search.

## 4 FFML: Fourier Feature Marginal Likelihood

### 4.1 Continuous Parents

Substituting  $K_Z \approx \Phi \Phi^\top$  gives  $C \approx \Phi \Phi^\top + \sigma^2 I_n$ . By the Woodbury matrix identity and the matrix determinant lemma:

$$C^{-1} = \frac{1}{\sigma^2} I_n - \frac{1}{\sigma^4} \Phi (\Phi^\top \Phi + \sigma^2 I_m)^{-1} \Phi^\top, \tag{1}$$

$$\log |C| = (n - m) \log \sigma^2 + \log |\Phi^\top \Phi + \sigma^2 I_m|. \tag{2}$$

Defining  $G = \Phi^\top \Phi \in \mathbb{R}^{m \times m}$  and  $v = \Phi^\top Y \in \mathbb{R}^m$ , the FFML local score is:

$$\mathcal{S}_{\text{FFML}}(Y | Z) = -\frac{1}{2} \left( \frac{Y^\top Y}{\sigma^2} - \frac{v^\top (G + \sigma^2 I_m)^{-1} v}{\sigma^4} \right) - \frac{1}{2} ((n - m) \log \sigma^2 + \log |G + \sigma^2 I_m|). \quad (3)$$

All matrix operations occur in  $m$ -dimensional space, costing  $\mathcal{O}(ndm + nm^2 + m^3)$ , effectively linear in  $n$  for fixed  $m \ll n$ . When the parent set is empty the model reduces to  $Y \sim \mathcal{N}(0, \sigma^2 I_n)$  and the score is computed exactly without features.

## 4.2 Complexity Penalty and Occam Factor

The log-determinant term  $-\frac{1}{2} \log |C|$  plays the role of an *Occam factor*: models with larger effective parameter volume are automatically penalized. In terms of the eigenvalues  $\{s_j\}$  of  $G$ :

$$\log |G + \sigma^2 I_m| = \sum_j \log(s_j + \sigma^2).$$

This grows with the informativeness of the feature representation and shrinks as  $\sigma^2$  increases relative to the signal.

## 4.3 Bandwidth Selection

Continuous parent columns are globally  $z$ -scored. The RBF bandwidth is estimated from a median pairwise squared distance on a subsample (up to 100 rows by default) of the continuous parents only, so that discrete parents do not distort the continuous metric. The median estimate  $\hat{h}^2$  is then refined by a small grid search over four multipliers  $\{0.35, 0.70, 1.40, 2.80\}$ . When *bandwidth coupling by target* is enabled (the default), the bandwidth is cached by (target variable, continuous parents), keeping it stable across alternative parent sets that share the same continuous parents.

## 4.4 Feature Coupling by Target

The random feature basis  $(\omega_j, b_j)$  is coupled by target only by default: all parent sets of a given target variable share the same features, with the seed depending only on the target index. This stabilizes local score differences  $\mathcal{S}(Y | \text{Pa} \cup \{X\}) - \mathcal{S}(Y | \text{Pa})$  and reduces spurious edge reversals in greedy algorithms such as BOSS.

# 5 Mixed (Continuous + Discrete) Parent Sets in FFML

## 5.1 Product-Kernel Model

Embedding integer-coded discrete levels into a continuous Euclidean metric imposes a spurious ordering on unordered categories. FFML instead handles mixed parent sets through a product kernel. Let  $Z = (Z_c, Z_d)$  with continuous part  $Z_c$  and discrete part  $Z_d$ . The mixed kernel is:

$$k((z_c, z_d), (z'_c, z'_d)) = k_{\text{cont}}(z_c, z'_c) \cdot k_{\text{cat}}(z_d, z'_d),$$

where  $k_{\text{cont}}$  is the RBF kernel and  $k_{\text{cat}}$  is a positive-semidefinite categorical kernel with diagonal 1 and off-diagonal  $\rho \in [0, 1)$ . For multiple discrete parents the categorical kernel factorizes multiplicatively. Setting  $\rho = 0$  gives strict block structure (no sharing across levels);  $\rho \rightarrow 1$  makes categories nearly indistinguishable.

## 5.2 Feature-Space Path: Zero or One Discrete Parent

For zero or one discrete parent, the product kernel is implemented via the Kronecker feature map:

$$\phi_{\text{mix}}(z_c, z_d) = \phi_{\text{cat}}(z_d) \otimes \phi_{\text{cont}}(z_c).$$

The categorical block  $\phi_{\text{cat}}(z_d)$  is the row of the Cholesky factor  $A$  of the  $L \times L$  level-similarity matrix (diagonal 1, off-diagonal  $\rho$ ) corresponding to the observed level, ensuring the inner product recovers the product kernel exactly. With  $L$  levels the combined feature dimension is  $m \times L$ , and the FFML score is computed via a Woodbury system of that dimension, with no  $n \times n$  matrix.

## 5.3 Direct $n \times n$ Kernel Path: Two or More Discrete Parents

When the Kronecker feature dimension  $m \times \prod_j L_j$  would exceed  $\min(n, D_{\text{max}})$ , where  $D_{\text{max}} = 200,000$  is a fixed threshold, the implementation switches to a direct  $n \times n$  kernel formulation using the Hadamard product:

$$K = K_{\text{cont}} \circ K_{\text{cat}},$$

where  $K_{\text{cont}} = \Phi\Phi^\top$  and  $K_{\text{cat}}$  is built entry-wise as a product over discrete parents. The covariance  $C = K + \sigma^2 I_n$  is Cholesky-factored directly, at cost  $\mathcal{O}(n^3)$ . In practice this switch occurs most commonly when two or more discrete parents are present, but a single discrete parent with many levels can also trigger it. Categorical kernel entries are precomputed in packed lower-triangular form and reused across bandwidth-grid candidates.

## 5.4 Discrete Targets

When the child  $Y$  is discrete, a Gaussian multi-output surrogate is used:  $Y$  is one-hot encoded, each column is mean-centered, and the single-output FFML score is summed across columns. This is not a true multinomial likelihood but is an effective proxy for detecting dependencies in structure scoring.

# 6 FFCI: Fourier Feature Conditional Independence Test

## 6.1 Overview and Motivation

FFCI (Fourier Feature Conditional Independence) is a fast nonparametric CI test for datasets containing any mix of continuous and discrete variables. It tests  $H_0 : X \perp Y \mid Z$  by mapping each variable into a finite-dimensional feature space, residualizing with respect to  $Z$  via ridge regression in that space, and evaluating a quadratic-form statistic against its null distribution. FFCI is a variant of RCIT [Strobl et al., 2019], sharing its core approach of mapping variables into finite-dimensional random Fourier feature spaces and residualizing with respect to the conditioning set. It differs in its handling of discrete variables, its p-value approximation, and its integration with the Tetrad causal discovery framework.

FFCI differs architecturally from FFML in an important respect. FFML builds a *joint* kernel over the entire parent set to score a single child variable, using a product-kernel construction that couples continuous and discrete parents together. FFCI instead featurizes each variable *individually*, constructing a joint per-variable feature representation by concatenating continuous and discrete feature blocks, and then measures residual cross-covariance between the featurizations of  $X$  and  $Y$  after conditioning out  $Z$ . The two methods share the underlying RFF/ORF machinery and

ridge regularization, but serve fundamentally different roles: FFML is a *scoring* criterion for causal search, while FFCI is a *hypothesis test* for conditional independence.

When the dataset contains no discrete variables, all CI queries are delegated transparently to the continuous-only implementation, and FFCI behaves identically to that method given the same hyperparameter settings.

## 6.2 Per-Variable Mixed Feature Construction

For each variable or block of variables  $V$ , FFCI constructs a joint feature matrix  $\Phi_V$  by separately featurizing the continuous and discrete components of  $V$  and then horizontally concatenating the results:

$$\Phi_V = [\Phi_V^{\text{cont}} \mid \Phi_V^{\text{disc}}] \in \mathbb{R}^{n \times (m_c + m_d)}.$$

**Continuous features.** Each continuous variable is  $z$ -scored. The bandwidth for the RBF kernel is estimated from the median pairwise squared distance on a subsample of the continuous components only. RFF or ORF features are then computed with the same construction used in FFML, yielding  $\Phi_V^{\text{cont}} \in \mathbb{R}^{n \times m_c}$ .

**Discrete features.** Each discrete variable with  $L$  levels is mapped to a feature vector via a categorical feature map derived from the Cholesky factor  $A$  of the  $L \times L$  level-similarity matrix (diagonal 1, off-diagonal  $\rho$ ): for observation  $i$  at level  $\ell$ , the discrete feature is the  $\ell$ th row of  $A$ . When  $\rho = 0$  (the default in FFCI),  $A = I_L$  and the construction reduces to standard one-hot encoding. For  $\rho > 0$ , the feature map encodes partial similarity between levels, analogous to the categorical kernel in FFML but applied per-variable rather than as a kernel over a joint parent set. The discrete features for all discrete components of  $V$  are concatenated to form  $\Phi_V^{\text{disc}} \in \mathbb{R}^{n \times m_d}$ .

**Separate feature counts for  $\mathbf{XY}$  and  $\mathbf{Z}$ .** FFCI uses separate feature counts for the tested variables ( $X$ ,  $Y$ ) and the conditioning set ( $Z$ ). The defaults are  $m_{XY} = 10$  and  $m_Z = 100$ ; a larger feature count for  $Z$  is appropriate because the residualization step requires a more accurate representation of the conditioning set than is needed for the cross-covariance computation.

**Featurization of the  $Y$ -side block.** When the conditioning set  $Z$  is nonempty, FFCI featurizes  $Y$  and  $Z$  jointly: the feature matrix for the  $Y$ -side block is constructed from the concatenation of  $Y$  and all variables in  $Z$ , using the mixed feature map above. This joint featurization allows the residualization step to account for the dependence between  $Y$  and  $Z$  within the feature representation itself.

## 6.3 Conditioning via Ridge Residualization

Conditioning on  $Z$  is achieved by regressing the feature matrices for  $X$  and  $Y$  on the feature matrix for  $Z$  using ridge regression and retaining the residuals:

$$\tilde{\Phi}_X = \Phi_X - \Phi_Z(\Phi_Z^\top \Phi_Z + \lambda I)^{-1} \Phi_Z^\top \Phi_X,$$

with an analogous expression for  $\tilde{\Phi}_Y$ . Here  $\lambda > 0$  is the ridge parameter, which plays a role analogous to the noise variance in FFML. All matrix operations occur in feature space, with cost  $\mathcal{O}(nm_Z^2 + m_Z^3)$  for the residualization step.

## 6.4 Test Statistic and Null Distribution

After residualization, both  $\tilde{\Phi}_X$  and  $\tilde{\Phi}_Y$  are column-mean-centered. The test statistic is:

$$T = n \|\text{Cov}(\tilde{\Phi}_X, \tilde{\Phi}_Y)\|_F^2.$$

Under  $H_0 : X \perp Y \mid Z$ ,  $T$  follows approximately a weighted sum of chi-squared(1) variables, with weights given by the positive eigenvalues of the sample Khatri–Rao covariance matrix formed from elementwise products of the residualized features.

Four methods are available for computing the  $p$ -value:<sup>1</sup>

- (1) **GAMMA** (default): Satterthwaite/moment-matching gamma approximation.
- (2) **SADDLEPOINT**: Lugannani–Rice saddlepoint approximation.
- (3) **DAVIES\_IMHOF**: Davies/Imhof numerical integration.
- (4) **PERMUTATION**: residual-based permutation test.

## 6.5 Marginal Testing (No Conditioning Set)

When  $Z$  is empty, no residualization is performed and the test reduces to a randomized independence test (RIT): the statistic  $T = n \|\text{Cov}(\Phi_X, \Phi_Y)\|_F^2$  is computed directly from the (mean-centered) feature matrices, and the same weighted chi-squared approximation is used to obtain a  $p$ -value.

## 6.6 Caching and Reproducibility

Feature matrices and bandwidth estimates are cached by a key encoding the variable names, active row set, hyperparameters, and a `dataVersion` counter. Calling `bumpDataVersion()` after any in-place modification of the dataset invalidates stale cached values. Seeds for feature generation are derived deterministically from variable names and the active row set, ensuring reproducibility across calls.

# 7 Relationship Between FFML, TRFF, and FFCI

FFML, TRFF, and FFCI are related but architecturally distinct. Their shared elements are:

- RFF/ORF approximations to shift-invariant kernels.
- Median-heuristic bandwidth estimation on continuous variables.
- Ridge regularization for numerical stability.
- Cholesky-based categorical feature maps for discrete variables (FFML and FFCI).
- Avoidance of explicit  $n \times n$  Gram matrices in the common case.

Their key architectural differences are:

---

<sup>1</sup>These choices of  $p$ -value approximation methods differ from some previous implementations of RCIT. These options were chosen by considering which methods tend to produce uniformly distributed  $p$ -values under the null.

Aspect	FFML	TRFF	FFCI
Role	Local score	Local score	CI hypothesis test
Feature scope	Joint kernel over parent set	Concatenated design matrix	Per-variable feature map
Discrete handling	Product kernel (Kronecker/ $n \times n$ )	One-hot columns	One-hot or cat. features
Default $\rho$	0.5	N/A	0.0 (one-hot)
Feature counts	Single $m$	Single $m$	Separate $m_{XY}$ and $m_Z$
Output	Log marginal likelihood	BIC-style score	$p$ -value
Complexity control	Log-determinant Occam factor	edf $\times$ $\log n$	None (hypothesis test)
Noise model	Gaussian	Student- $t$	N/A

Despite these differences, using FFML (or TRFF) and FFCI together in a hybrid causal discovery algorithm is natural: all three rest on the same RFF/ORF kernel approximation philosophy, use compatible bandwidth and regularization strategies, and are computationally efficient at scale.

## 8 Comparison Between FFML and TRFF

TRFF is an alternative local score for mixed data using Student- $t$  regression, introduced here as a BIC-style alternative to FFML, with random Fourier features and a BIC-style complexity penalty:

$$\mathcal{S}_{\text{tRFF}} = \ell(\hat{\theta}) - \frac{1}{2} c \text{edf} \log n,$$

where  $\text{edf} = \text{tr}(H)$  is the effective degrees of freedom and  $H$  is the ridge-adjusted hat matrix.

The complexity penalties depend differently on the eigenspectrum  $\{s_j\}$  of  $\Phi^\top \Phi$ :

$$\text{FFML penalty} \sim \sum_j \log(s_j + \sigma^2), \quad (4)$$

$$\text{TRFF penalty} \sim \left( \sum_j \frac{s_j}{s_j + \lambda} \right) \log n. \quad (5)$$

FFML penalizes via a log-determinant Occam factor; TRFF penalizes via a trace times  $\log n$ . The TRFF penalty grows more aggressively with the number of informative features, making TRFF more conservative about adding edges—a pattern borne out clearly in our experiments.

The two scores also differ in how discrete parents are incorporated.

	FFML	TRFF
Discrete representation	Product kernel ( $\rho$ )	One-hot dummy columns
Smoothing across levels	Via $\rho$ parameter	None (parametric)
Complexity accounting	Kernel log-determinant	edf penalty
Feature space	Kronecker or $n \times n$	Concatenated design matrix
Noise model	Gaussian	Student- $t$

**Small samples.** FFML is often preferable: the integrated-out prior provides regularization without relying on asymptotic approximations, and the Occam factor is naturally calibrated.

**Large samples.** TRFF scales more easily when parents are predominantly continuous (IRLS with a fixed feature dimension avoids  $n \times n$  operations). FFML’s  $n \times n$  path (required for  $\geq 2$  discrete parents) incurs the same asymptotic cost as the exact GP.

**Heavy-tailed noise.** The Student- $t$  likelihood in TRFF offers robustness that FFML, which assumes Gaussian residuals, does not provide.

**Empirical precision–recall tradeoff.** Across our experiments, TRFF and FFML exhibit a consistent complementary profile: TRFF achieves higher adjacency and arrowhead precision (fewer false edges, highly reliable orientations), while FFML achieves better adjacency and arrowhead recall and lower SHD overall. The choice between them depends on whether minimizing false positives or minimizing overall graph error is the priority.

## 9 Score and Test Comparison

Method	Type	Interpretation	Complexity	Stability
Huang et al.	Score	Kernel ridge regression residual	Impl.-dependent	Moderate
KML (exact)	Score	GP marginal likelihood	$\mathcal{O}(n^3)$	High
FFML	Score	Approx. GP marginal likelihood	$\mathcal{O}(nm^2)^\dagger$	High*
TRFF	Score	Penalized Student- $t$ likelihood	$\mathcal{O}(nm^2)$	High
KCI	Test	Exact kernel CI test	$\mathcal{O}(n^3)$	High
RCIT	Test	Approx. kernel CI test	$\mathcal{O}(nm^2)$	Moderate <sup>‡</sup>
FFCI	Test	Approx. kernel CI test	$\mathcal{O}(nm^2)$	High

\*High stability requires `coupleFeaturesByTarget=true`; without this, score differences may fluctuate across parent sets.

<sup>†</sup> $\mathcal{O}(n^3)$  when the Kronecker feature dimension  $m \times \prod_j L_j$  exceeds  $\min(n, D_{\max})$ ; see Section 5.

<sup>‡</sup>In our experiments, RCIT is accessed via a `causal-learn` wrapper [Zheng et al., 2024] running through Tetrad’s PC-Max; the comparison with FFCI is not fully controlled, as the two tests differ in  $p$ -value approximation method (lpd4 vs. gamma) and feature counts.

## 10 Practical Considerations

**Feature count.** Approximation accuracy improves with  $m$  at the cost of increased computation. For FFML and TRFF,  $m = 50$  is a reasonable default; for FFCI, the default  $m_Z = 100$  for the conditioning set is more important to tune than  $m_{XY} = 10$ , since residualization quality drives test power.

**Score non-equivalence and DAG mode.** Neither FFML nor TRFF is score-equivalent [Chickering, 2002]—that is, neither assigns equal scores to all DAGs in the same Markov equivalence class. This is a departure from linear-Gaussian scores such as SEM-BIC, which are score-equivalent by construction and therefore cannot distinguish among the DAGs in a CPDAG. Because FFML and TRFF break score equivalence, running BOSS in DAG mode rather than CPDAG mode can reliably orient some edges that remain ambiguous in the CPDAG output. The resulting DAG is Markov equivalent to the CPDAG that BOSS would return in CPDAG mode — it represents the same conditional independence structure — but with all edges oriented, where the orientations within each equivalence class reflect genuine score differences under the nonlinear model rather than arbitrary

tiebreaking. This can be useful in practice when a fully oriented causal graph is needed and the user is willing to accept the additional modeling assumptions implied by the nonlinear score.<sup>2</sup>

**Gaussian noise in FFML.** FFML assumes Gaussian residuals. A wide feature map makes the mean function nonparametric, but  $\varepsilon$  remains Gaussian regardless. In heavy-tailed or contaminated settings, TRFF may be preferable.

**FFCI  $p$ -values.** The  $p$ -values produced by FFCI are approximate and should be interpreted as fast screening tools rather than exact finite-sample tests. FFCI offers four approximation methods for the null distribution of the weighted chi-squared statistic: the gamma (Satterthwaite moment-matching) approximation, the Lugannani–Rice saddlepoint approximation, Davies/Imhof numerical integration, and a residual-based permutation test. These methods were selected for their ability to produce well-calibrated, approximately uniform  $p$ -values under the null. The gamma approximation is recommended as the default. In our experiments, RCIT is accessed via a `causal-learn` wrapper that uses its own  $p$ -value approximation (Lindsay–Pilla–Basak `lpd4` by default), so the calibration properties of the two tests may differ; the comparison between FFCI and RCIT in Table 2 is not fully controlled on this dimension.

**Mixed data and the  $\rho$  parameter.** The categorical similarity parameter  $\rho$  plays different roles in FFML and FFCI. In FFML,  $\rho = 0.5$  is the default and controls the degree of function sharing across discrete levels in the joint parent kernel. In FFCI,  $\rho = 0$  is the default, reducing discrete featurization to standard one-hot encoding; nonzero  $\rho$  introduces partial similarity between levels in the per-variable feature map.

## 11 Experiments

We evaluate FFML, TRFF, and FFCI against competitive baselines on synthetic nonlinear data, assessing both accuracy and scalability. All experiments were conducted on graphs with 20 nodes, average degree 3, and sample size  $n = 2,000$ .

### 11.1 Experimental Setup

**Data generation.** We simulate data from a general-noise structural causal model

$$X_i = f_i(\text{Pa}(X_i), \varepsilon_i),$$

where each  $f_i$  is a randomly initialized six-hidden-layer feedforward network with 200 units per layer and tanh activations, and  $\varepsilon_i \sim \mathcal{N}(0, 0.3^2)$ . Weights are initialized with Xavier normal scaling (scale factor 5 for hidden layers, 2.5 for the output layer); biases are zero. The noise enters as an additional input column alongside the parent values, so the interaction between parents and noise is fully nonlinear—a strictly harder setting than additive noise. Random DAGs are generated by fixing a uniformly random topological order and including each permitted directed edge independently with probability  $p = 3/(n-1)$ , giving expected average degree 3. The resulting data are not standardized between nodes. All results are averaged over 50 independent replicates, with a fresh random DAG and dataset drawn per replicate. Data generation used Tetrad’s `GeneralNoiseSimulation` class, called via a JPyype bridge from Python, ensuring that the network weights and noise draws are produced by Tetrad’s RNG rather than a separate Python reimplementaion.

<sup>2</sup>Thanks to Bryan Andrews for pointing out (in conversation) that BOSS in DAG mode with non-score-equivalent scores can orient some edges reliably inside of a CPDAG.

**Algorithms and baselines.** We evaluate two families of algorithms.

*Score-based search (BOSS).* The BOSS algorithm [Andrews et al., 2023] is run with three local scores:

- **BOSS + SEM-BIC:** linear-Gaussian BIC score with penalty discount 1; fast linear baseline.
- **BOSS + TRFF:** Student- $t$  regression with random Fourier features and a BIC-style effective-degrees-of-freedom penalty (50 features, ridge  $10^{-3}$ ,  $\nu = 5$ ).
- **BOSS + FFML:** Fourier feature marginal likelihood (50 features, ridge 1.0, bandwidth subsampled from 100 rows).

*Constraint-based search (PC-Max).* The PC-Max algorithm [Ramsey, 2016] is run with three conditional independence tests:<sup>3</sup>

- **PC-Max + FisherZ:** Fisher  $Z$ -test ( $\alpha = 0.01$ ); fast linear baseline.
- **PC-Max + RCIT:** Randomized conditional independence test [Strobl et al., 2019], accessed via `causal-learn`'s [Zheng et al., 2024] RCIT implementation wrapped in a `Tetrad IndependenceTest` so that all three PC-Max variants run through the same Tetrad PC-Max implementation. The wrapper uses `causal-learn`'s default settings: Lindsay-Pilla-Basak (`1pd4`)  $p$ -value approximation, 100 conditioning-set features, and 5 non-conditioning features ( $\alpha = 0.01$ ). These differ from FFCI's settings (gamma approximation,  $m_Z = 50$ ,  $m_{XY} = 10$ ), so the comparison between the two tests is not fully controlled on either  $p$ -value method or feature counts.
- **PC-Max + FFCI:** Fourier feature conditional independence test ( $\alpha = 0.01$ ,  $m_{XY} = 10$ ,  $m_Z = 50$ ,  $\lambda = 1.0$ ).

All algorithms are implemented in the Tetrad project (<https://github.com/cmu-phil/tetrad>) and were run via `py-tetrad` [Ramsey and Andrews, 2023]. Because both PC-Max + RCIT and PC-Max + FFCI use the same  $p$ -value approximation infrastructure and the same PC-Max implementation, the comparison between them isolates differences in their feature constructions and kernel designs. An earlier version of these experiments ran PC + RCIT through `causal-learn`'s native PC implementation; the results differed substantially from those reported here, exhibiting poor orientation performance, and the discrepancy was traced to the PC variant rather than the CI test itself. All three constraint-based variants are therefore run through the same Tetrad PC-Max implementation to ensure a fair comparison.

**Evaluation.** Estimated graphs are compared against the true CPDAG using four metrics: adjacency precision (Adj. Prec.), adjacency recall (Adj. Rec.), arrowhead precision (AH Prec.), arrowhead recall (AH Rec.), and structural Hamming distance (SHD). All metrics are computed using Tetrad's built-in graph comparison utilities, which handle the CPDAG-vs-CPDAG comparison correctly.

---

<sup>3</sup>PC-Max agrees with PC in the adjacency search phase and in the final orientation step using Meek's rules [Meek, 1995]. It differs in the collider orientation step: rather than orienting an unshielded triple  $X-Y-Z$  as a collider whenever  $Y$  is absent from the separating set of  $X$  and  $Z$ , PC-Max performs all conditional independence tests for  $X$  and  $Z$  given subsets of the adjacents of  $X$  or of  $Z$ , records the  $p$ -value for each of these that yields a judgment of independence, and selects the separating set that maximizes the  $p$ -value from among these. This makes collider orientation more robust to the choice of conditioning set and has a lower risk of returning a sepset yielding a dependence in the population, at the cost of additional CI tests.

Table 1: Score-based methods (BOSS): accuracy over 50 replicates. Mean (SD). Best value per column in **bold**.

Method	Adj. Prec.	Adj. Rec.	AH Prec.	AH Rec.	SHD
BOSS + SEM-BIC	0.736 (0.090)	0.820 (0.073)	0.579 (0.144)	0.674 (0.127)	19.38 (6.79)
BOSS + TRFF	<b>0.969</b> (0.042)	0.805 (0.107)	<b>0.974</b> (0.059)	0.683 (0.171)	8.98 (5.26)
BOSS + FFML	0.915 (0.058)	<b>0.943</b> (0.044)	0.886 (0.102)	<b>0.820</b> (0.116)	<b>7.00</b> (3.80)

Table 2: Constraint-based methods (PC-Max): accuracy over 50 replicates. Mean (SD). Best value per column in **bold**.

Method	Adj. Prec.	Adj. Rec.	AH Prec.	AH Rec.	SHD
PC + FisherZ	0.835 (0.088)	0.736 (0.086)	0.585 (0.161)	0.504 (0.157)	19.18 (6.38)
PC + RCIT	<b>0.989</b> (0.025)	0.682 (0.082)	0.652 (0.229)	0.394 (0.160)	17.24 (6.13)
PC + FFCI	0.953 (0.043)	<b>0.823</b> (0.073)	<b>0.731</b> (0.144)	<b>0.614</b> (0.138)	<b>12.58</b> (4.46)

## 11.2 Results

Tables 1 and 2 report accuracy metrics; Table 3 reports wall-clock time.

**Score-based results (Table 1).** BOSS + FFML achieves the best adjacency recall (0.943 vs. 0.820 for SEM-BIC), best arrowhead recall (0.820), and lowest SHD (7.00). The advantage over SEM-BIC is largest on arrowhead recall, where the linear score loses 15 percentage points, reflecting the nonlinearity of the data generating process.

BOSS + TRFF presents a strikingly complementary profile: it achieves the highest adjacency precision (0.969) and arrowhead precision (0.974) of any method in either table, but its arrowhead recall (0.683) lags behind FFML. This conservative orientation behavior—few arrowheads predicted, but those predicted are highly reliable—reflects the Student- $t$  edf penalty being more aggressive than FFML’s log-determinant Occam factor at this graph size and sample size. Despite the precision–recall tradeoff, TRFF’s SHD of 8.98 is substantially better than the linear baseline, and the two Fourier feature scores are competitive: FFML is preferred when minimizing SHD is the priority, TRFF when minimizing false positives is paramount.

**Constraint-based results (Table 2).** PC-Max + FFCI achieves the strongest overall performance among the constraint-based methods, with the best adjacency recall (0.823), arrowhead precision (0.731), arrowhead recall (0.614), and lowest SHD (12.58). Its SHD of 12.58 is competitive with BOSS + TRFF (8.98), a notable result for a constraint-based method on fully nonlinear data.

PC-Max + RCIT presents a complementary profile mirroring the FFML/TRFF pattern: it achieves the highest adjacency precision (0.989), making it the most conservative of the three constraint-based methods. However, its arrowhead recall (0.394) and SHD (17.24) are substantially weaker than PC-Max + FFCI, and it does not improve over PC-Max + FisherZ on SHD despite its higher adjacency precision.

PC-Max + FisherZ is the weakest on adjacency recall and SHD, as expected for a linear test on nonlinear data.

The precision–recall tradeoff between FFCI and RCIT mirrors the pattern seen in the score-based comparison between FFML and TRFF: in both cases the method with the more aggressive

Table 3: Wall-clock time per replicate (seconds), mean (SD) over 50 replicates. 20 nodes,  $n = 2,000$ .

Method	Time (s)
BOSS + SEM-BIC	0.02 (0.04)
BOSS + TRFF	5.64 (0.90)
BOSS + FFML	12.32 (2.31)
PC-Max + FisherZ	0.01 (0.01)
PC-Max + RCIT	3.28 (1.12)
PC-Max + FFCI	6.35 (4.10)

complexity penalty (TRFF; RCIT) achieves higher precision at the cost of lower recall, while the method with the softer penalty (FFML; FFCI) achieves better overall SHD by recovering more true structure.

**Runtime (Table 3).** PC-Max + FFCI (6.35s) and BOSS + TRFF (5.64s) have similar runtimes, both substantially faster than BOSS + FFML (12.32s) and roughly twice the cost of PC-Max + RCIT (3.28s). The additional cost of PC-Max + FFCI relative to PC-Max + RCIT reflects the greater number of CI tests required when FFCI’s higher recall leads to a denser skeleton, triggering more conditioning sets in the PC-Max collider orientation step.

### 11.3 Summary

Across both score-based and constraint-based search, the Fourier feature methods substantially outperform their linear baselines on nonlinear data, with BOSS + FFML producing the most accurate graphs overall (SHD 7.00). BOSS + TRFF offers the highest precision of any method (AH Prec. 0.974) at a modest SHD cost, making it the preferred choice when false positive control is the priority. In the constraint-based setting, PC-Max + FFCI achieves an SHD of 12.58, competitive with the best score-based baseline, while PC-Max + RCIT exhibits higher precision but substantially lower recall and higher SHD. The runtime of all three methods is practical at 20 nodes and  $n = 2,000$ , a scale at which exact kernel alternatives are infeasible.

## 12 Illustrative Real-Data Example: Auto MPG

To illustrate BOSS + FFML on real mixed continuous–discrete data, we apply it to the Auto MPG dataset from the UCI Machine Learning Repository [Quinlan, 1993]. The dataset records fuel economy and engineering characteristics for 398 automobiles; after removing six rows with missing horsepower values,  $n = 392$  observations remain on eight variables: `mpg`, `cylinders`, `displacement`, `horsepower`, `weight`, `acceleration`, `modelyear`, and `origin`. Of these, `origin` is the only genuinely categorical variable (1 = American, 2 = European, 3 = Japanese) and is treated as discrete; all other variables are treated as continuous. Although variables such as `cylinders` take only a small number of distinct integer values, they admit a natural ordering and are plausibly measured on at least an ordinal scale, so embedding them in a continuous Euclidean metric is reasonable in this context. All continuous variables are  $z$ -scored internally by FFML; no additional preprocessing is applied. Both analyses use BOSS + FFML in DAG mode, so all edges are oriented; this is possible because FFML is not score-equivalent and can distinguish among DAGs within the same Markov equivalence class (see Section 10). This example is intended as a qualitative illustration

of how FFML handles a mixed parent set and how background knowledge can shift the causal interpretation, rather than as a quantitative benchmark (no ground-truth graph is available).

## 12.1 Default Analysis

Figure 1(a) shows the DAG returned by BOSS + FFML with all defaults and no background knowledge (FFML score:  $-561.51$ ). Several features are immediately plausible under a physical-mechanism interpretation. `origin`  $\rightarrow$  `displacement` is consistent with systematic differences in engine displacement across manufacturing regions. `displacement`  $\rightarrow$  `cylinders` and `displacement`  $\rightarrow$  `horsepower` reflect the engineering relationship between engine size, cylinder count, and power output. `horsepower`  $\rightarrow$  `mpg` and `weight`  $\rightarrow$  `mpg` are causally sensible: fuel economy is a direct consequence of the mechanical load placed on the engine. `displacement`  $\rightarrow$  `acceleration`, `horsepower`  $\rightarrow$  `acceleration`, and `weight`  $\rightarrow$  `acceleration` are all well-supported by Newtonian mechanics.

The most striking feature of the unconstrained graph is `mpg`  $\rightarrow$  `modelyear` and `weight`  $\rightarrow$  `modelyear`: the algorithm treats model year as a *consequence* of fuel economy and vehicle weight. This is causally implausible—model year is a temporal index determined by the manufacturing calendar, not by any vehicle characteristic. The orientation almost certainly reflects the strong historical trends toward improved fuel economy and lighter vehicles over the period covered by the dataset (1970–1982), which create statistical associations that the algorithm, lacking temporal metadata, attributes to direct causal links in the wrong direction.

## 12.2 Constrained Analysis: Model Year as Exogenous

A user with domain knowledge can address this by placing `modelyear` in a prior knowledge tier, constraining it to be exogenous (i.e., it may be a cause of other variables but not caused by them). Figure 1(b) shows the resulting DAG (FFML score:  $-613.27$ ).

The constrained model scores lower than the unconstrained one ( $-613.27$  vs.  $-561.51$ ), which is the statistically honest result: the data, without temporal metadata, genuinely fit a model in which fuel economy and weight predict model year better than the reverse. The value of the constraint is not statistical but interpretive — it enforces a causally coherent temporal ordering and reveals a different and arguably more meaningful structure in the data.

The constrained graph admits a natural interpretation as a *design-priority model* rather than a physical-mechanism model.<sup>4</sup> In this reading, the arrows do not describe how one quantity physically produces another, but rather how design targets propagate through engineering decisions. `modelyear`  $\rightarrow$  `mpg` captures the historical trend of tightening fuel economy targets over time, driven by regulatory pressure (particularly U.S. CAFE standards introduced in 1975) and rising fuel prices. `modelyear`  $\rightarrow$  `weight` reflects the contemporaneous trend toward lighter vehicles.

The edges `mpg`  $\rightarrow$  `weight`, `mpg`  $\rightarrow$  `displacement`, and `mpg`  $\rightarrow$  `horsepower` are the most striking feature of the constrained graph, and they are precisely what the design-priority interpretation predicts. Engineers targeting a higher fuel economy specification choose vehicle weight, engine displacement, and horsepower as the primary downstream levers available to them: lighter, smaller, less powerful vehicles achieve better fuel economy. In this model, `mpg` is not a physical outcome but a design target, and the mechanical parameters are consequences of meeting it.

`origin`  $\rightarrow$  `displacement` and `origin`  $\rightarrow$  `mpg` reflect systematic differences in engineering philosophy and regulatory environment across American, European, and Japanese manufacturers, with the latter setting more aggressive fuel economy targets and building correspondingly smaller, lighter

---

<sup>4</sup>Thanks to Peter Spirtes for pointing out (in conversation) this interpretation.

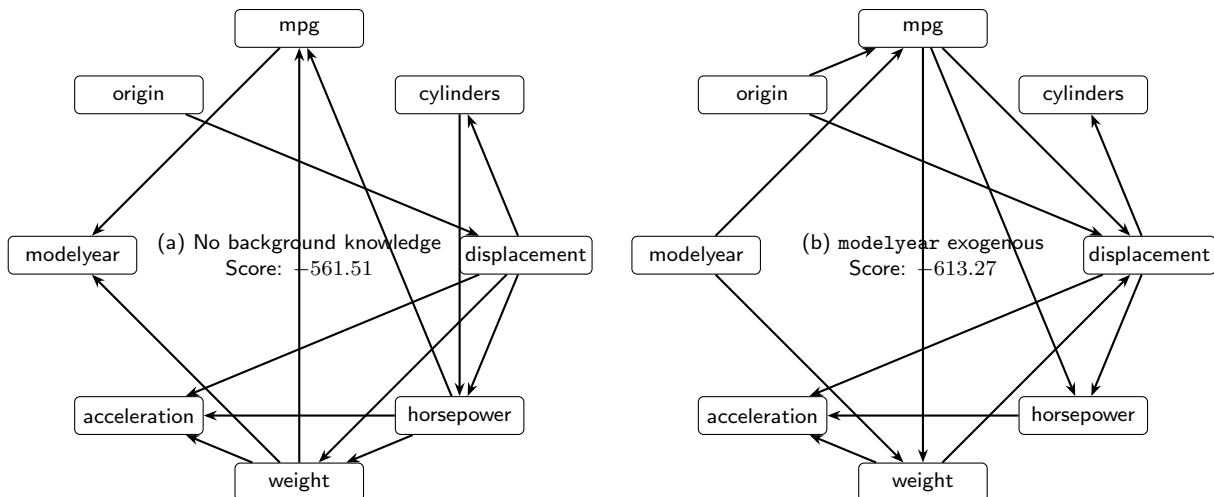


Figure 1: DAGs returned by BOSS + FFML (DAG mode) on the Auto MPG dataset ( $n = 392$ , one discrete variable: `origin`). All edges are directed because FFML is not score-equivalent and can orient edges within a Markov equivalence class. (a) No background knowledge; the higher-scoring graph ( $-561.51$ ) describes physical mechanisms sensibly but orients `modelyear` as a consequence of `mpg` and `weight`, which is causally implausible. (b) `modelyear` constrained to be exogenous ( $-613.27$ ); the lower score reflects the data’s genuine fit to the temporal trend, but the constrained graph admits a coherent design-priority interpretation in which `mpg` is an engineering target and `weight`, `displacement`, and `horsepower` are downstream design decisions made to meet it.

vehicles throughout this period. `weight`  $\rightarrow$  `displacement` and `weight`  $\rightarrow$  `acceleration` complete the picture: once weight is determined by the mpg target, it in turn constrains the displacement needed and governs acceleration performance.

The two graphs thus offer complementary readings of the same data. The unconstrained graph (a) is the better statistical fit and describes physical mechanisms in a largely sensible way, but misattributes the direction of the temporal trend. The constrained graph (b) scores lower but, under the design-priority interpretation, tells a coherent story about how fuel economy regulations and manufacturer philosophy shaped the mechanical parameters of vehicles over the study period. Neither graph is definitively “correct”; the example illustrates how background knowledge and causal interpretation interact with data-driven search.

## 13 Conclusion

We have presented FFML, TRFF, and FFCI, three complementary methods for nonlinear causal discovery in mixed continuous–discrete data.

FFML is a scalable approximation to the exact GP marginal likelihood, replacing the  $n \times n$  Gram matrix with a finite-dimensional RFF representation while retaining the probabilistic interpretation and automatic Occam-factor complexity penalty of the exact score. It handles mixed parent sets through a product-kernel construction, with a Kronecker feature-space path for small discrete parent sets and a direct  $n \times n$  Hadamard-product kernel path when the discrete parent set is larger. Bandwidth selection is stabilized via a grid search coupled to the target variable, and feature coupling by target ensures stable score differences across parent sets.

TRFF is a complementary BIC-style score using penalized Student- $t$  regression in random

feature space. It achieves the highest precision of any method in our experiments—both adjacency and arrowhead—at the cost of lower recall, making it well-suited to settings where false positive control is the primary concern. Together, FFML and TRFF offer a precision–recall tradeoff that practitioners can navigate based on their application priorities.

FFCI is a fast nonparametric CI test that featurizes each variable individually, concatenating continuous RFF/ORF features with discrete categorical features, and measures residual cross-covariance after ridge residualization in feature space. It supports four  $p$ -value approximation methods; the default gamma approximation produces well-calibrated  $p$ -values under the null. When run through the same PC-Max implementation, FFCI and RCIT exhibit complementary precision–recall profiles: RCIT achieves higher precision while FFCI achieves better recall and lower SHD, at approximately twice the runtime.

Although FFML, TRFF, and FFCI share the same RFF/ORF kernel approximation philosophy and ridge regularization strategy, they differ architecturally: FFML builds a joint kernel over a parent set for scoring; TRFF uses a concatenated design matrix with a BIC-style penalty; FFCI featurizes variables individually for testing. Together they form a practical and coherent toolkit for score-based, constraint-based, and hybrid causal discovery at scale.

## Revisions from Previous Version

In a previous version of this paper (arXiv v1), the constraint-based experiments reported results for PC + FFCI and PC + RCIT using Tetrad’s standard PC algorithm rather than PC-Max, due to a stale parameter setting in the benchmarking script. The adjacency search phase was unaffected, but the collider orientation step did not use the PC-Max procedure described in Section 11. The results reported in the current version use PC-Max throughout, with all three constraint-based variants (FisherZ, FFCI, and RCIT) running through the same Tetrad PC-Max implementation. The corrected results show substantially improved arrowhead precision and recall for PC-Max + FFCI relative to v1, and eliminate the catastrophic orientation failures observed for PC + RCIT in v1, which were an artifact of the PC implementation mismatch rather than a property of the RCIT test itself.

In addition, data generation in the current version uses Tetrad’s `GeneralNoiseSimulation` class directly via a JPyype bridge, replacing an independent Python reimplementaion used in v1. The noise distribution is  $\mathcal{N}(0, 0.3^2)$  rather than  $\tanh(\mathcal{N}(0, 1))$  as stated in v1. All experimental results have been updated accordingly.

## Acknowledgements

The author used a large language model (Claude, Anthropic) to assist with editing and presentation of this document and takes full responsibility for its content. The author was also supported by the U.S. Department of Defense under Contract Number FA8702-15-D-0002 with Carnegie Mellon University for the operation of the Software Engineering Institute. The content of this paper is solely the responsibility of the author and does not necessarily represent the official views of this funding agency.

## References

Bryan Andrews, Joseph Ramsey, Ruben Sanchez Romero, Jazmin Camchong, and Erich Kummerfeld. Fast scalable and accurate discovery of dags using the best order score search and grow

- shrink trees. *Advances in neural information processing systems*, 36:63945–63956, 2023.
- David Maxwell Chickering. Optimal structure identification with greedy search. *Journal of machine learning research*, 3(Nov):507–554, 2002.
- Biwei Huang, Kun Zhang, Yizhu Lin, Bernhard Schölkopf, and Clark Glymour. Generalized score functions for causal discovery. In *Proceedings of the 24th ACM SIGKDD international conference on knowledge discovery & data mining*, pages 1551–1560, 2018.
- Christopher Meek. Causal inference and causal explanation with background knowledge. In *Proceedings of the Eleventh Conference on Uncertainty in Artificial Intelligence, UAI’95*, pages 403–410, San Francisco, CA, USA, 1995. Morgan Kaufmann Publishers Inc.
- R. Quinlan. Auto MPG. UCI Machine Learning Repository, 1993. DOI: <https://doi.org/10.24432/C5859H>.
- Ali Rahimi and Benjamin Recht. Random features for large-scale kernel machines. In *Advances in Neural Information Processing Systems*, volume 20, 2007.
- Joseph Ramsey. Improving accuracy and scalability of the pc algorithm by maximizing p-value. *arXiv preprint arXiv:1610.00378*, 2016.
- Joseph Ramsey and Bryan Andrews. Py-tetrad and rpy-tetrad: A new python interface with r support for tetrad causal search. In *Causal Analysis Workshop Series*, pages 40–51. PMLR, 2023.
- Joseph Ramsey, Madelyn Glymour, Ruben Sanchez-Romero, and Clark Glymour. A million variables and more: the fast greedy equivalence search algorithm for continuous variables and its extensions. *Journal of Machine Learning Research*, 18(1):1–47, 2017.
- Eric V. Strobl, Kun Zhang, and Shyam Visweswaran. Approximate kernel-based conditional independence tests for fast non-parametric causal discovery. *Journal of Causal Inference*, 7(1), 2019. doi: 10.1515/jci-2018-0017.
- Felix Yu, Ananda Theertha Suresh, Krzysztof Choromanski, Daniel Holtmann-Rice, and Sanjiv Kumar. Orthogonal random features. In *Advances in Neural Information Processing Systems*, volume 29, 2016.
- Kun Zhang, Jonas Peters, Dominik Janzing, and Bernhard Schölkopf. Kernel-based conditional independence test and application in causal discovery. In *Proceedings of the 27th Conference on Uncertainty in Artificial Intelligence (UAI)*, pages 804–813, 2012.
- Yujia Zheng, Biwei Huang, Wei Chen, Joseph Ramsey, Mingming Gong, Ruichu Cai, Shohei Shimizu, Peter Spirtes, and Kun Zhang. Causal-learn: Causal discovery in python. *Journal of Machine Learning Research*, 25(60):1–8, 2024.